New chemical tools to illuminate N-acylphosphatidylethanolamine biosynthesis

Wendel, T.J.

5

Development of an activity-based probe that visualizes cellular PLA2G4E activity

One of the important aspects of molecular biology is acquiring an understanding of the spatiotemporal function of enzymes.[1,2] Genetic abrogation of enzyme expression, such as accomplished with CRISPR-Cas9, is useful to investigate enzyme functions due to its high target specificity[3], but does not provide temporal control and may disrupt multiple functionalities of the target because it completely removes a protein from the biological system.[4–6] Inhibitors allow acute modulation of enzyme activity, which enables the study of the physiological function of an enzyme in a dynamic fashion.[5,7] Because inhibitors may have multiple cellular targets, evidence of a direct interaction between the inhibitor molecule and the protein of interest, referred to as 'target engagement', is critical to assign the phenotypic effects observed to the studied enzyme.[8–10] In drug discovery, proof of target engagement in combination with a desired phenotypic effect is important to validate the protein as a drug target.[8,11,12] In addition, information about the drug concentration needed for full target engagement may help to determine the maximal dose required for efficacy with minimal side-effects.[8,13]

Activity-based protein profiling (ABPP) has become one of the key methodologies to determine enzyme activity in a physiological setting and can be used for target engagement studies.[14,15] ABPP makes use of an activity-based probe (ABP) that covalently engages with the catalytic residue and is equipped with a fluorescent or biotin reporter tag for visualization and identification purposes, respectively (Figure 5.1).[16,17] In a 'two-step labeling' approach, selective ligation of the probe to its reporter tag is executed after sample treatment to minimize the interference of a large reporter group with the probe's activity and cell permeability (Figure 5.1).[18] In competitive ABPP, pre-treatment of samples with an inhibitor prevents the binding of the ABP, leading to a dose-dependent decrease in labeling. This provides evidence of target engagement by the inhibitor in cells and allows to determine its potency and selectivity in a single experiment.[19–21] Competitive ABPP is, therefore, a powerful method to investigate these critical drug properties in early drug discovery.

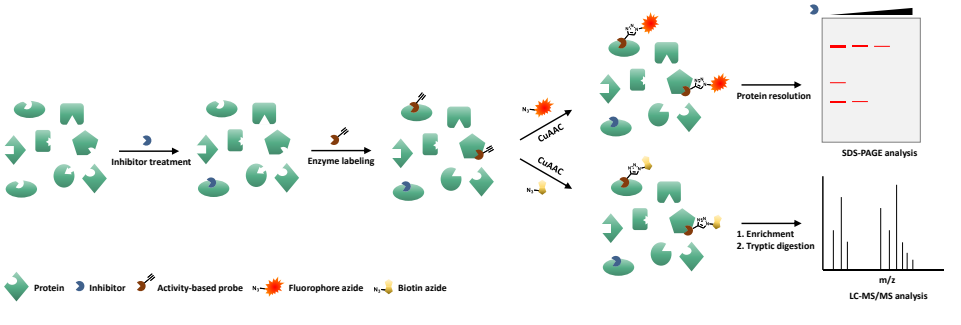

Figure 5.1. Schematic overview of competitive ABPP workflow. Cells or lysate are treated with inhibitor, followed by activity-based alkyne probe. After lysis, copper-catalyzed alkyne-azide cycloaddition (CuAAC) is used to attach a reporter group. SDS-PAGE and subsequent in-gel fluorescence scanning or probe target enrichment via biotin-streptavidin pulldown in combination with LC-MS/MS are used to analyze labeled enzymes.

PLA2G4E is a 868 amino acid (100 kDa) serine hydrolase (SH) that is one of the six known members of the group IV phospholipases (PLA2G4A–F).[22,23] These enzymes share common structural characteristics that include an N-terminal calcium-dependent lipid binding domain (C2) and a catalytic Ser-Asp dyad, which are important for their subcellular localization and catalytic activity.[24,25] PLA2G4E has an additional C-terminal polybasic domain (KKKRLK) which is involved in its localization.[26] While PLA2G4A–F all metabolize phospholipids, they have different activities, substrate preferences and expression patterns.[23,24,27] In 2016, PLA2G4E was reported to be an *N*-acyltransferase capable of producing *N*-acylphosphatidylethanolamines (NAPEs) from phosphatidylethanolamine (PE) and phosphatidylcholine (PC) in a calcium-dependent manner.[28] NAPEs are a low-abundant class of lipids that have both signaling and structural functionalities. They are involved in regulation of satiety[29] and have anti-inflammatory properties.[30] In addition, they modulate membrane dynamics by providing stability and stimulating fusion.[31–33] Via several pathways, NAPE hydrolysis leads to the formation of *N*-acylethanolamines (NAEs), a highly diverse family of signaling lipids.[34–39] Depending on the nature of their fatty acid substituent, NAEs are involved in a wide range of bioactivities, including nociception, anxiety, fertility, appetite, inflammation and memory formation.[40–47]

In previous chapters, competitive ABPP was applied to the discovery of inhibitors for PLA2G4E, using broad-spectrum serine hydrolase probe fluorophosphonate-tetramethylrhodamine (FP-TAMRA). **WEN091** was identified as a potent inhibitor of PLA2G4E *in vitro* (pIC_{50} ± SEM = 8.01 ± 0.02, Chapter 2), which was able to reduce NAPE levels in a cellular PLA2G4E overexpression system and showed cellular activity on other serine hydrolases (Chapter 3). To confirm the physical, intracellular interaction between **WEN091** and PLA2G4E, a cell-permeable ABP targeting PLA2G4E is required. Here, the design and synthesis of ABP **1** and its application to study the cellular target engagement of **WEN091** is described.

Results

Design and synthesis of ABP 1

The broad reactivity of FP-TAMRA and its charged fluorophore that compromises its cell permeability made this probe not suitable for cellular engagement studies.[48,49] Therefore, a new probe was required to study the cellular target engagement of PLA2G4E inhibitors. It was envisioned that compound **2**, a PLA2G4E inhibitor identified in Chapter 4, could serve as starting point for the design of a cell-permeable probe (Figure 5.2A). The electrophilic carbonyl of **2** is thought to bind to the catalytic serine of PLA2G4E and the triazole functions as a leaving group (Figure 5.2B). The benzylpiperidine acts as a 'staying group' and irreversibly carbamoylates the serine. Modification of the benzylpiperidine with a ligation handle would, therefore, allow visualization of the active enzyme by conjugation to a fluorescent reporter group. A commonly used ligation strategy involves bioorthogonal Huisgen 1,3-dipolar cycloaddition ('click' chemistry) of an azide and an alkyne, often

catalyzed by copper (also referred to as CuAAC).[49] It was envisioned that an alkyne could be incorporated at the *meta* position of the benzyl group, since substitution at this position was tolerated by PLA2G4E (e.g. compound **3**, Figure 5.2A, see also Chapter 2).

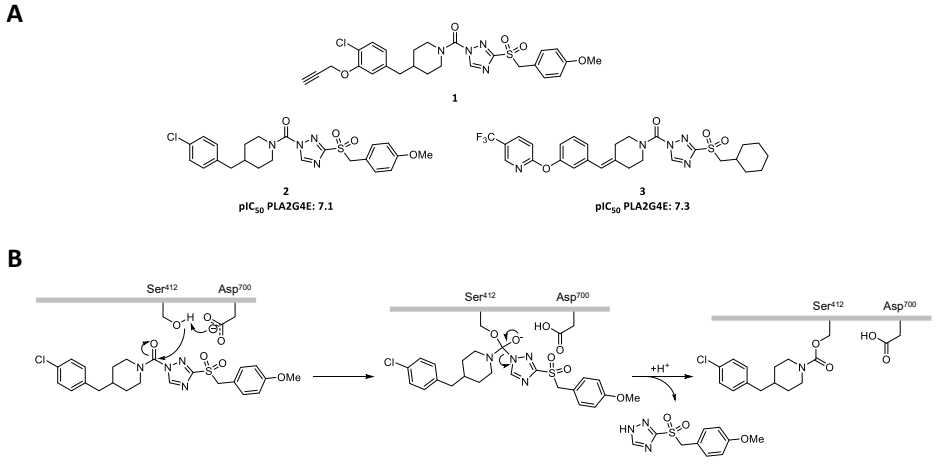

Figure 5.2. Rationale of the design of PLA2G4E probe 1. A) The design of **1** was based on the chemical structure of inhibitors **2** and **3**. pIC_{50} values were determined with gel-based ABPP on PLA2G4E-HEK293T lysate. B) Hypothesized mechanism of PLA2G4E inhibition by **2**. PLA2G4E's nucleophilic residue Ser^{412} is activated by Asp^{700} and attacks the electrophilic carbonyl of **2**. The triazole moiety leaves, forming a stable adduct of the piperidine moiety on PLA2G4E.

Synthesis of ABP **1** was started with construction of benzylpiperidine **4** from 4-methylenepiperidine **5** and 2-chloro-5-iodophenol (**6**) via Suzuki-Miyaura cross-coupling (Scheme 5.1). Installation of the propargyl group (**7**) and Boc-deprotection yielded the piperidinium salt (**8**). In a parallel route, 1*H*-1,2,4-triazole-3-thiol (**9**) was benzylated with 4-methoxybenzyl chloride (**10**) to form **11** and subsequently oxidated with peracetic acid to sulfone **12**. Triphosgene-mediated urea formation between piperidine **8** and triazole **12** finally afforded ABP **1**.

Biological characterization of PLA2G4E ABP 1

1 is an activity-based probe for PLA2G4E

The ability of **1** to inhibit PLA2G4E was assessed in a competitive ABPP experiment using FP-TAMRA. Briefly, PLA2G4E-overexpressing HEK293T cell lysate was treated with **1** at increasing concentrations (30 min), followed by FP-TAMRA (50 nM, 5 min). Sodium dodecyl sulfate-polyacrylamide gel electrophoresis (SDS-PAGE) and in-gel fluorescence scanning enabled determination of the apparent half maximal inhibitory concentration (IC_{50}) of **1** to be 54 nM (pIC_{50} ± SEM = 7.27 ± 0.02, Figure 5.3A, B). Of note, **1** did not inhibit overexpressed recombinant PLA2G4B–D up to 1–10 µM (Figure 5.3C). To confirm the fluorescent labeling of PLA2G4E by **1**, overexpression lysate was treated with **1** (1 µM, 30 min), followed by copper-catalyzed click conjugation of Cy5-azide to **1**. Resolution of the

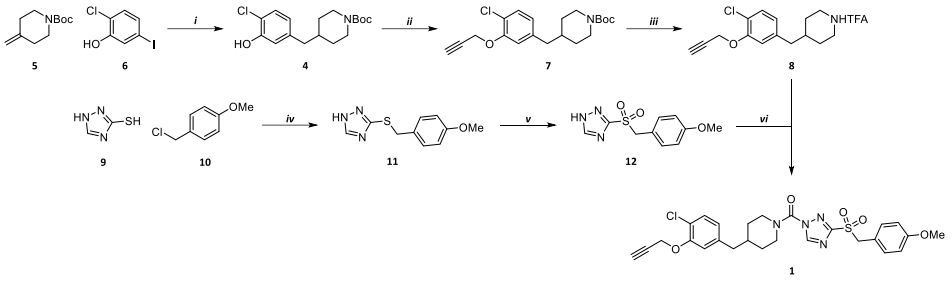

Scheme 5.1. Synthesis of 1. Reagents and conditions: *i*) 1. **5**, 9-BBN, THF, 6 h 0°C → RT, then 2. **6**, K_2CO_3, Pd(dppf)Cl_2, THF:DMF:H_2O (1:1:0.1), o/n 60°C (84%); *ii*) Propargyl bromide, K_2CO_3, DMF, 48 h RT (quant.); *iii*) TFA, DCM, 21 h RT; *iv*) K_2CO_3, DMF, 5 h RT; *v*) AcOOH, DCM, o/n 0°C → RT (90%); *vi*) 1. **8**, triphosgene, DIPEA, THF, o/n 0°C → RT, then 2. **12**, K_2CO_3, DMF, o/n RT (48%).

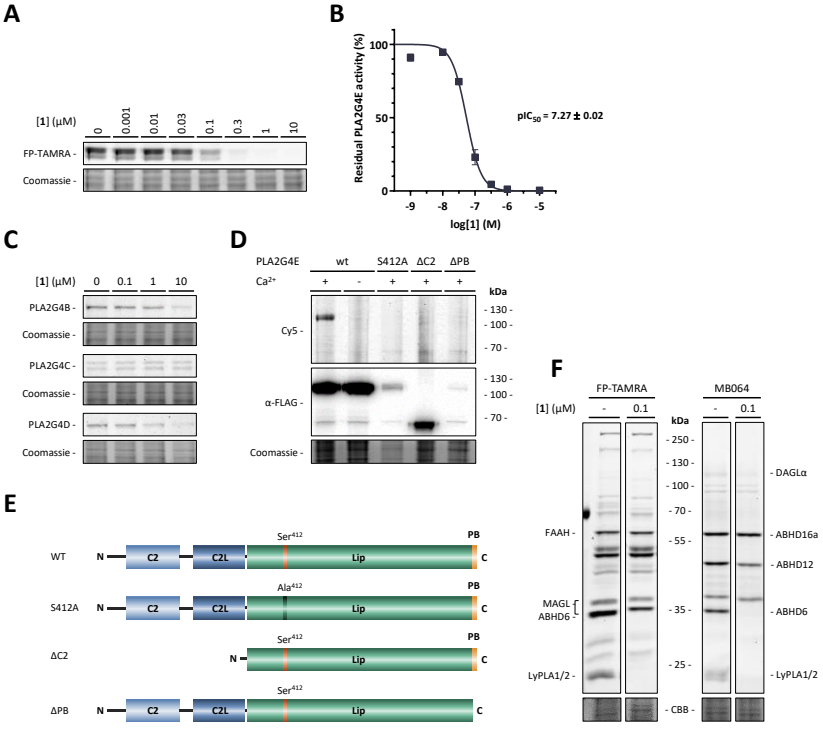

Figure 5.3. Activity of 1 on PLA2G4E and related enzymes. A) Representative gel excerpts of ABPP experiments on PLA2G4E overexpression lysate, using FP-TAMRA as ABP. B) Corresponding inhibition curve and pIC_{50} value. Data reported as mean ± SEM (N = 3). C) Representative gel excerpts of ABPP experiments on PLA2G4B, PLA2G4C and PLA2G4D overexpression lysate, using FP-TAMRA as ABP. D) Activity-based labeling of recombinantly overexpressed wt and mutant PLA2G4E by 1 (1 μM). Excerpts of fluorescence image after CuAAC conjugation to Cy5, western blot and coomassie loading control. E) Schematic representation of PLA2G4E wt and mutant constructs used in this study, indicating the calcium-dependent lipid binding domain (C2), the C2-like domain (C2L), the lipase domain (Lip) with nucleophilic residue Ser^{412} and polybasic stretch (PB). F) Representative gel excerpts of ABPP experiments on mouse brain membrane proteome, using FP-TAMRA and MB064 as ABPs.

proteins by SDS-PAGE and fluorescence scanning showed a fluorescent band at the expected MW of PLA2G4E (Figure 5.3D, first lane). No labeling was observed in the absence of Ca^{2+} (Figure 5.3D, second lane) or when the catalytic serine was mutated to an alanine (S412A) (third lane), indicating that labeling of PLA2G4E by **1** is dependent on its catalytic activity. In addition, mutants in which the C2 domain (ΔC2) or polybasic domain (ΔPB) were removed were not labeled by **1** (Figure 5.3D, E). This confirms and extends previous reports that these mutants were not active in a substrate-based assay.[50] Altogether, these results demonstrate that **1** can be used as an ABP to visualize the PLA2G4E activity.

The selectivity of **1** over other serine hydrolases was investigated using competitive ABPP on mouse brain membrane proteome as reported in Chapter 3. **1** (100 nM, 30 min) inhibited several other serine hydrolases, including α/β-hydrolase domain-containing protein 6 (ABHD6), diacylglycerol lipase α (DAGLα) and protein thioesterases 1 and 2 (LyPLA1/2), while it partially inhibited ABHD12 (Figure 5.3F). NAE-degrading enzyme fatty acid amide hydrolase (FAAH) and monoacylglycerol lipase (MAGL) were not inhibited. Thus, compound **1** is a potent PLA2G4E ABP with limited serine hydrolase off-targets in mouse brain proteome.

Cellular activity of probe 1 confirmed *in situ* target engagement of inhibitor WEN091

The activity of **1** in a cellular system was investigated using mouse neuroblastoma cell line Neuro-2a. In brief, Neuro-2a cells were transiently transfected with recombinant human PLA2G4E or mock plasmid. The cells were incubated with **1** at various concentrations for 30 min, harvested and lysed. The resulting homogenate was subjected to CuAAC using Cy5-azide followed by SDS-PAGE to enable visualization of PLA2G4E labeling. With increasing concentration of **1**, a band at the MW of PLA2G4E was fluorescently labeled in overexpressing cells, but not in mock (Figure 5.4A). This indicated **1** was able to engage with and label PLA2G4E in the overexpressing cells. Of note, a second band (~37 kDa) is dose-dependently labeled, but also in mock. This probably indicated engagement of **1** with an off-target protein in Neuro-2a cells. Thus, **1** is a cellular active ABP that can be used to visualize the intracellular activity of PLA2G4E.

Next, Neuro-2a cells overexpressing PLA2G4E were pre-treated with inhibitor **WEN091** (30 min) followed by treatment with **1** (1 μM, 30 min). Cells were then lysed and the resulting homogenate was subjected to CuAAC. **WEN091** dose-dependently inhibited labeling of PLA2G4E by **1** (pIC_{50} = 6.47 ± 0.19, Figure 5.4C, D) achieving full inhibition at 10 μM. These results proved the intracellular engagement of **WEN091** with PLA2G4E.

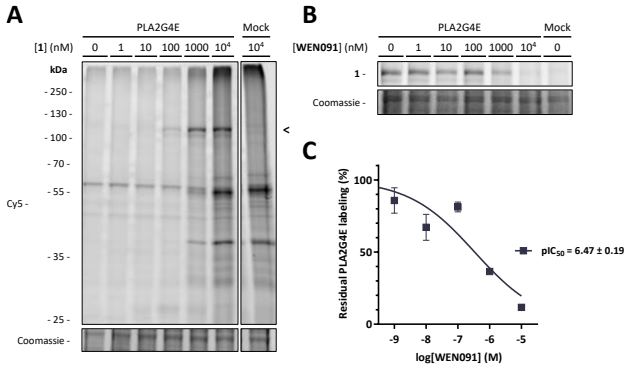

Figure 5.4. Activity on and labeling of PLA2G4E in Neuro-2a cells by ABP 1. A) Labeling of PLA2G4E- and mock-transfected Neuro-2a cells by **1** (30 min). **1** was clicked to Cy5-N_3 after cell lysis. Band of PLA2G4E is indicated with an arrow. B) Intracellular PLA2G4E labeling by **1** (1 µM, 30 min) is dose-dependently outcompeted by **WEN091** (30 min). **1** was clicked to Cy5-N_3 after cell lysis. C) Corresponding inhibition curve and pIC_{50} value of **WEN091**. Data reported as mean ± SEM (N = 4).

Discussion and conclusions

In drug discovery, cellular target engagement studies are important to correlate the phenotypic effects of an inhibitor to its presumed mode of action. It helps to validate the protein as a drug target and provides information about the dose required for full target occupancy.[10,12,13] **WEN091** was identified as a nanomolar potent inhibitor of PLA2G4E in biochemical assays (Chapter 2), but lowered (lyso)-NAPE levels in PLA2G4E-overexpressing Neuro-2a cells only at micromolar concentrations (Chapter 3). This discrepancy may suggest that **WEN091** has restricted cell permeability and/or limited engagement with PLA2G4E in a cellular setting. Here, cellular PLA2G4E ABP **1** (**WEN175**) was developed to address this question.

Compound **1** was able to label PLA2G4E in a dose-dependent manner. It did not label PLA2G4E in the absence of calcium, demonstrating the activity-dependent nature of the probe. Furthermore, it did not label PLA2G4E-S412A, confirming Ser^{412} to be the catalytic residue.[50] **1** was able to visualize cellular PLA2G4E activity, and using **1**, it was determined that **WEN091** intracellularly engaged with PLA2G4E with pIC_{50} = 6.47 ± 0.17. This shows that **WEN091** is cell-permeable, but that it is more than 30-fold less potent in a cellular setting. Full target engagement was achieved at 10 µM, which is in line with the lipidomics measurements that showed (lyso)-NAPE reduction at >10 µM (Chapter 3). High cellular levels of substrates PE and PC that compete for interaction with PLA2G4E may explain this reduced activity of **WEN091** in cells.[51] These results also indicate that biochemical assays *in vitro* may overestimate a compound's activity and emphasize the importance of cellular target engagement assays to guide the development of inhibitors.

Projecting forward, ABP **1** can potentially be used to detect endogenous PLA2G4E activity in cells and tissues and to investigate its activity under (patho)physiological conditions. For example, NAPEs are highly elevated in ischemic tissue, possibly as a cytoprotective mechanism.[52–54] It is envisioned that **1** could be employed to visualize PLA2G4E activity under normal and ischemic conditions using chemical proteomics to investigate the role of PLA2G4E in this process. Calcium-independent NAPE producing enzymes phospholipase A/acyltransferase (PLAAT) 1 and PLAAT5 share a similar expression profile to PLA2G4E.[55,56] Quantification of PLA2G4E activity using ABP **1** will help to elucidate the contribution of PLA2G4E to NAPE production in healthy and ischemic tissue. Visualizing the subcellular localization of active PLA2G4E using **1** and a fluorescent reporter tag may show whether PLA2G4E, similar to PLA2G4A, translocates before activation.[57–59] The C2 domain is thought to regulate the subcellular localization of PLA2G4 family members and to be involved in enzyme activity through interactions with substrate lipids in cellular membranes.[57–60] PLA2G4E's PB domain was previously demonstrated to be involved in the enzyme's localization towards membranes of the endocytic recycling machinery.[26] Here, however, both the C2 and PB domain were needed for probe binding in lysate, indicating a more direct involvement of these domains in PLA2G4E's activity.

A drawback of ABP **1** is that it targets multiple other serine hydrolases, which might hamper the identification of endogenous PLA2G4E using gel-based ABPP or microscopy. Future optimization of this chemical series may lead to more specific probes suitable for microscopy experiments.

In conclusion, we report **1** as the first cell-permeable activity-based probe that was used to confirm the intracellular activity of PLA2G4E in an overexpression system and to prove intracellular target engagement of PLA2G4E inhibitor **WEN091**.

Acknowledgements

Lian van den Berg, Sanne Uitenbroek, Hans den Dulk and Tom van der Wel are kindly acknowledged for plasmid cloning and purification, Hans van den Elst for HRMS analysis.

Experimental procedures

General remarks

All chemicals and reagents for biochemical experiments were purchased from Thermo Fisher Scientific or Bio-Rad, unless noted otherwise. Activity-based probes were purchased from Thermo Fisher Scientific (FP-TAMRA) or synthesized in-house (MB064)[21].

Plasmids

The full-length cDNA of wild type human PLA2G4E (GenScript Biotech), murine PLA2G4B, hPLA2G4C and mPLA2G4D (Source BioScience) were cloned into a pcDNA™3.1(+) expression vector in-frame with a C-terminal FLAG tag. PLA2G4E mutants were generated by PCR amplification using the primers listed in Supplementary Table S5.1. Purified PCR products were cloned into pcDNA™3.1(+) in-frame with a C-terminal FLAG tag. Plasmids were isolated from transformed *Escherichia coli* XL-10 using a Qiagen Plasmid Midi kit and stored at 4°C in TE buffer (10 mM Tris, 0.1 mM EDTA, pH 8.0). The sequence was determined (Macrogen) and verified using CLC Main Workbench.

Supplementary Table S5.1. Oligonucleotides used for generating PLA2G4E mutant constructs.

Construct name	Direc.	Sequence	Restriction site used
PLA2G4E-S412A	fw	5′-ATCGTCTCACCGGTATGAGTCTCCAGGCCTCGGAAGGC-3′	Kpn2I
	rev	5′-CATCTCTAGACTACGTACGCTCGAGCTTATCGTCGTCATCCTTGTAATC-3′	Pfl23II
PLA2G4E-ΔC2	fw	5′-CATGGTACCGCCACCATGGTGCGGCTGGGCTTCAGCCT-3′	Acc65I
	rev	5′-CATCTCTAGACTACGTACGCTCGAGCTTATCGTCGTCATCCTTGTAATC-3′	XhoI
PLA2G4E-ΔPB	fw	5′-CTTAAGCTTTACCGGTACCGCCACCATGAGTCTCCAGGCCTCGGAAGGC-3′	Acc65I
	rev	5′-CTACGTACGCTCGAGCTTATCGTCGTCATCCTTGTAATCCTCCACTGCGAGCCGCAGAGCC-3′	XhoI

Cell culture

HEK293T (human embryonic kidney) and Neuro-2a (murine neuroblastoma) cells (ATCC) were cultured in Dulbecco's Modified Eagle's Medium (DMEM, Sigma-Aldrich D6546) with additional heat-inactivated new-born calf serum (10% (v/v), Avantor Seradigm), L-Ala-L-Gln (2 mM, Sigma-Aldrich), penicillin and streptomycin (both 200 µg/mL, Duchefa Biochemie) at 37°C, 7% CO_2. Medium was refreshed every 2–3 days and cells were passaged twice a week at 70–80% confluence by aspirating the medium, thorough pipetting in fresh medium and seeding to appropiate density. Cell cultures were regularly tested for mycoplasma and discarded after 2–3 months.

HEK293T membrane preparation

One day prior to transfection, 10^7 HEK293T cells were seeded to a 15 cm dish. Upon transfection, medium was aspirated and replaced by 13 mL fresh medium. Plasmid DNA (20 µg per 15 cm dish) and PEI (60 µg per 15 cm dish) were separately dissolved in 1 mL DMEM without serum per dish, combined, incubated for 15 min and added dropwise to the cells. 24 h p.t. medium was replaced by 25 mL fresh medium. 72 h p.t. medium was aspirated and the cells were washed with RT Dulbecco's PBS (DPBS, Sigma-Aldrich D8537), harvested in DPBS and centrifuged (3000 × *g*, 15 min, RT). Cell pellets were flash-frozen in liquid N_2 and stored at −80°C until use.

HEK293T cell pellets were thawed on ice and homogenized in 2 mL ice-cold lysis buffer (50 mM Tris-HCl, 2 mM DTT, 1 mM $MgCl_2$, 5 U/mL Benzonase® (Santa Cruz Biotechnology, Inc.), pH 8.0 with additional 3 mM $CaCl_2$ for PLA2G4E) per 15 cm cell culture dish using a Sonics® Vibra-Cell VCX 130 probe sonicator equipped with a 2 mm microtip (3 × 10 s on/10 s off, 20% amplitude). After incubation on ice for 30 min the insoluble ("membrane") fraction was separated from the soluble ("cytosol") fraction by ultracentrifugation (10^5 × *g*, 35 min, 4°C, Beckman-Coulter ultracentrifuge, Ti70.1 rotor).

The pellet was resuspended in 1 mL ice-cold storage buffer (50 mM Tris-HCl, 2 mM DTT, pH 8.0 with additional 3 mM $CaCl_2$ for PLA2G4E) per 15 cm plate and homogenized by passing through an insulin needle. After determination of the protein concentration using a Quick Start™ Bradford Protein Assay (Bio-Rad) the samples were diluted to 1.0 mg/mL in ice-cold storage buffer, aliquoted to single-use volumes, flash-frozen in liquid N_2 and stored at −80°C until further use.

Mouse brain lysate preparation

For ABPP experiments, mouse brains were harvested from surplus C57Bl/6J mice (8–14 weeks old) according to guidelines approved by the ethical committee of Leiden University (AVD1060020171144), immediately flash-frozen in liquid N_2 and stored at −80°C until use. Upon preparation, intact brains were thawed on ice and homogenized in 6 mL ice-cold lysis buffer (20 mM HEPES, 2 mM DTT, 250 mM sucrose, 1 mM $MgCl_2$, 25 U/mL Benzonase®, pH 6.8) using a Wheaton™ dounce homogenizer (DWK Life Sciences) and incubated on ice for 1 h. Cell debris was removed by low-speed centrifugation (170 × *g*, 5 min, 4°C), after which the supernatant was subjected to ultracentrifugation to separate membrane and cytosol fractions. The pellet was resuspended in ice-cold storage buffer (20 mM HEPES, 2 mM DTT, pH 6.8) and homogenized by passing through an insulin needle. The protein concentrations of both fractions were determined using a Quick Start™ Bradford Protein Assay and samples were diluted to 2.0 mg/mL (membrane) or 1.0 mg/mL (cytosol) using ice-cold storage buffer, aliquoted to single-use volumes, flash-frozen in liquid N_2 and stored at −80°C until use.

Activity-based protein profiling

HEK293T or mouse brain lysates were thawed on ice. 19.5 µL lysate was incubated with 0.5 µL inhibitor solution in DMSO (Sigma-Aldrich) for 30 min (RT), followed by addition of 0.5 µL probe in DMSO (PLA2G4E: FP-TAMRA, 50 nM, 5 min; PLA2G4B, PLA2G4C, PLA2G4D: FP-TAMRA, 500 nM, 20 min; mouse brain: FP-TAMRA, 500 nM, 20 min or MB064, 250 nM, 20 min, RT. Final DMSO concentration 5% (v/v)). The reaction was quenched by addition of 7 µL 4× Laemmli sample buffer (240 mM Tris, 8% (w/v) SDS, 40% (v/v) glycerol, 5% (v/v) β-mercaptoethanol (Sigma-Aldrich), 0.04% bromophenol blue) and incubation for 15 min at RT. 10 µL sample was resolved on 8% (PLA2G4E) or 10% (PLA2G4B, PLA2G4C, PLA2G4D, mouse brain) acrylamide SDS-PAGE gels (180 V, 75 min) and the gel was imaged on a Bio-Rad Chemidoc MP using Cy3/TAMRA settings (ex. 532/12 nm, em. 602/50 nm). Coomassie Brilliant Blue (CBB) R250 staining was used for total protein loading correction.

For ABPP on PLA2G4E mutants, 19.5 µL HEK293T overexpression lysate without DTT was treated with 0.5 µL **1** in DMSO for 30 min (RT), followed by addition of 2.2 µL freshly-prepared 'click mix' (*i.e.* 13 mM $CuSO_4$, 2.6 mM tris(3-hydroxypropyltriazolylmethyl)amine (THPTA), 95 µM Cy5-N_3 and 13 mM tris(2-carboxyethyl)phosphine (TCEP) combined in this order and mixed thoroughly). The ABPP mixture was shaken (800 rpm) for 30 min at 37°C, after which the reaction was quenched and proteins were resolved as described above. After imaging, proteins on the top half of the gel were transferred onto a 0.2 µM polyvinylidene fluoride (PVDF) membrane using a Trans-Blot Turbo Transfer system (Bio-Rad) and subsequently treated with anti-FLAG antibody (mouse, Sigma-Aldrich F3165) and horse radish peroxidase (HRP)-conjugated secondary antibody (m-IgGκ BP-HRP, Santa Cruz Biotechnology, Inc. sc-516102). Blots were developed using Clarity Western ECL Substrate (Bio-Rad). The bottom half of the gel was used for total protein loading correction using CBB. Images were analyzed using Bio-Rad Image Lab 6. IC_{50} calculations were performed in GraphPad Prism 7.

Cellular target engagement assay

Three days prior to the experiment, Neuro-2a cells were seeded to 12-wells plates plates (~$0.25 \cdot 10^6$ cells per well). One day later, medium was aspirated and replaced by 400 µL fresh medium. PLA2G4E or mock plasmid DNA (1 µg per well) and PEI (5 µg per well) were separatedly dissolved in 50 µL DMEM without serum per well, combined, incubated for 15 min and added dropwise to the cells. 24 h p.t., medium was replaced by 1 mL fresh medium per well. 48 h p.t., the experiment was started and medium was aspirated and cells were washed with RT DPBS. For competition experiments, 400 µL DMEM without serum with **WEN091** in DMSO (0.25% (v/v) DMSO) was added and cells were incubated for 30 min at 37°C. Medium was aspirated and 400 µL DMEM without serum with **1** in DMSO (0.25% (v/v) DMSO) was added and cells were incubated for 30 min at 37°C. Then medium was aspirated and cells were washed with RT DPBS. Cells were harvested in ice-cold DPBS by thorough pipetting and centrifuged (1000 × *g*, 6 min, RT). Pellets were flash-frozen in liquid N_2 and stored at −80°C until further use.

Cell pellets were thawed on ice and lysed in 50 µL lysis buffer (50 mM Tris-HCl, 2 mM DTT, 250 mM sucrose, 3 mM $CaCl_2$, 1 mM $MgCl_2$, 10 U/mL Benzonase®, pH 8.0). After incubation on ice for 20 min, the protein concentration was determined using Quick Start™ Bradford Protein Assay and the samples were diluted to 1.0 mg/mL using lysis buffer. 20 µL of this whole lysate was treated with 2 µL freshly prepared click mix (1.35 mM $CuSO_4$, 8.8 mM sodium ascorbate, 0.14 mM THPTA, 4.9 µM Cy5-N_3) and the mixture was incubated for 1 h at 37°C. Reactions were then quenched with 8 µL 4× Laemmli sample buffer and proteins were resolved and images analyzed as described under Activity-based protein profiling.

Organic synthesis

General remarks

All chemicals were purchased from Sigma-Aldrich, Combi-Blocks, Alfa Aesar or Fluorochem, common salts from Sigma-Aldrich or Chem-Lab and solvents from Sigma-Aldrich or Honeywell Riedel-de Haën and used without further purification. All moisture-sensitive reactions were carried out in solvents dried over heat-activated molecular sieves (4 Å, Sigma-Aldrich), using flame-dried glassware under an atmosphere of N_2. TLC analysis was performed on Merck silica gel 60 F_{254} aluminum TLC plates, on which compounds were visualized under 254 or 366 nm UV light and using $KMnO_4$ (30 mM $KMnO_4$, 180 mM K_2CO_3 in water) or ninhydrin (7.5 mM ninhydrin, 10% (v/v) AcOH in EtOH) stain. Flash column chromatography was performed using SiO_2 (Macherey-Nagel, 60 M) as stationary phase.

NMR spectra were recorded on a Bruker AV-400 MHz spectrometer at 400 MHz (^{1}H) and 101 MHz (^{13}C), using $CDCl_3$ or MeOD (Eurisotop) as solvent. Chemical shifts are reported in ppm with TMS (^{1}H $CHCl_3$, δ 0.00) or solvent resonance (^{1}H MeOD, δ 3.31; ^{13}C MeOD, δ 49.00; ^{13}C $CHCl_3$, δ 77.16) as internal standard. Data are reported as follows: chemical shift δ (ppm), multiplicity (s = singlet, d = doublet, t = triplet, dd = doublet of doublets, td = triplet of doublets, qd = quartet of doublets, dt = doublet of triplets, bs = broad singlet (^{1}H), br = broad (^{13}C), m = multiplet), coupling constants *J* (Hz) and integration. HPLC/MS analysis was performed on a Finnigan Surveyor HPLC system equipped with a Macherey-Nagel NUCLEODUR C_{18} Gravity, 5 µm, 50 × 4.6 mm column followed by a Thermo Scientific LTQ Orbitrap XL spectrometer, using H_2O/CH_3CN + 1% TFA as mobile phase. All compounds used for biological experiments were ≥ 95% pure based on LC/MS UV absorbance.

(4-(4-Chlorobenzyl)piperidin-1-yl)(3-((cyclohexylmethyl)sulfonyl)-1*H*-1,2,4-triazol-1-yl)-methanone (WEN091)

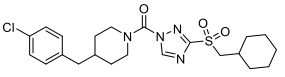

The title compound was synthesized as described in Chapter 2.

(4-(4-Chloro-3-(prop-2-yn-1-yloxy)benzyl)piperidin-1-yl)(3-((4-methoxybenzyl)sulfonyl)-1*H*-1,2,4-triazol-1-yl)methanone (1, WEN175)

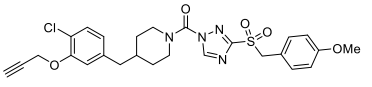

To an ice-cold solution of triphosgene (3 eq, 400 mg, 1.35 mmol) and DIPEA (3 eq, 234 µL, 1.34 mmol) in dry THF (5 mL), **9** (1 eq, 169 mg, 0.45 mmol) dissolved in dry THF (10 mL) was added dropwise over the course of 20 min. The mixture was stirred on ice for 1 h before it was allowed to warm to RT and stirred overnight. When TLC analysis confirmed full conversion the mixture was diluted with EtOAc and washed with water and brine. The organic layer was dried over $MgSO_4$, filtrated and concentrated *in vacuo*. Water was removed by co-evaporation with toluene, after which the resulting dark green oil was dissolved in dry DMF (6 mL). **13** (1.2 eq, 136 mg, 0.54 mmol) and K_2CO_3 (3 eq, 188 mg, 1.36 mmol) were added and the mixture was stirred overnight. The mixture was diluted with EtOAc and washed with water and brine. The organic layer was dried over $MgSO_4$, filtrated and concentrated *in vacuo*. Flash column chromatography (20 → 60% EtOAc in pentane) afforded the title compound as pale yellow sticky oil (117 mg, 0.22 mmol, 48%).

^{1}H NMR (400 MHz, $CDCl_3$) δ 8.84 (s, 1H), 7.28 (d, *J* = 8.0 Hz, 1H), 7.20 – 7.12 (m, 2H), 6.88 (d, *J* = 1.8 Hz, 1H), 6.83 – 6.76 (m, 2H), 6.74 (dd, *J* = 8.1, 1.8 Hz, 1H), 4.79 (d, *J* = 2.3 Hz, 2H), 4.55 (s, 2H), 4.42 – 4.26 (m, 1H), 4.15 – 3.94 (m, 1H), 3.70 (s, 2H), 2.98 – 2.83 (m, 2H), 2.67 (t, *J* = 2.4 Hz, 1H), 2.60 – 2.49 (m, 3H), 1.88 – 1.72 (m, 2H), 1.66 – 1.55 (m, 1H), 1.45 – 1.14 (m, 2H).

^{13}C NMR (101 MHz, $CDCl_3$) δ 160.50, 160.12, 152.62, 148.00, 146.94, 139.44, 132.14, 130.08, 122.83, 120.75, 118.06, 115.29, 114.19, 76.84, 76.60, 59.99, 56.63, 55.12, 47.06 (br), 45.98 (br), 42.20, 37.58, 31.50 (br).

HRMS: $[M+NH_4]^+$ calculated for $C_{26}H_{27}ClN_4O_5S$ $+NH_4^+$ 560.17289, found 560.17282.

***tert*-Butyl 4-(4-chloro-3-hydroxybenzyl)piperidine-1-carboxylate (4)**

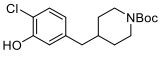

To an ice-cold solution of *N*-Boc 4-methylenepiperidine (**5**, 1 eq, 1.03 mL, 5.06 mmol) in degassed dry THF (20 mL), 9-BBN (1.4 eq, 14 mL 0.5 M in THF, 7.0 mmol) was added dropwise. The reaction was allowed to warm to RT and stirred for 6 h. In the meantime, a three-neck flask equipped with a reflux condenser was charged with K_2CO_3 (1.5 eq, 1.05 g, 7.60 mmol), 2-chloro-5-iodophenol (**6**, 1.6 eq, 2.0 g, 7.86), DMF (20 mL) and water (2 mL) and purged with N_2. When TLC analysis confirmed full conversion, the reaction mixture was added to the three-neck flask and purging was continued for 30 min. $Pd(dppf)Cl_2$ (0.01 eq, 37 mg, 0.051 mmol) was added, upon which the mixture turned dark red, and the reaction was stirred overnight at 60°C under continuous N_2 flow. The mixture was allowed to cool to RT, diluted with Et_2O and washed with 1 M aq. NaOH. The pH of the aqueous layer was neutralized with 12 M hydrochloric acid before the aqueous layer was extracted with Et_2O. The combined organic layers were washed with brine, dried over $MgSO_4$, filtrated and concentrated *in vacuo*. Flash column chromatography (0 → 35% EtOAc in pentane) afforded the title compound as off-white crystalline solid (1.38 g, 4.25 mmol, 84%).

^{1}H NMR (400 MHz, $CDCl_3$) δ 7.20 (d, *J* = 8.1 Hz, 1H), 6.80 (d, *J* = 2.0 Hz, 1H), 6.63 (dd, *J* = 8.1, 2.0 Hz, 1H), 4.17 – 4.03 (m, 3H), 2.69 – 2.58 (m, 2H), 2.45 (d, *J* = 6.9 Hz, 2H), 1.97 – 1.76 (m, 1H), 1.71 – 1.55 (m, 2H), 1.45 (s, 9H), 1.12 (qd, *J* = 13.0, 12.5, 3.9 Hz, 2H).
^{13}C NMR (101 MHz, $CDCl_3$) δ 155.08, 151.47, 140.99, 128.88, 122.04, 117.62, 116.97, 79.63, 44.03, 42.67, 38.05, 31.97, 28.57.

tert-Butyl 4-(4-chloro-3-(prop-2-yn-1-yloxy)benzyl)piperidine-1-carboxylate (7)

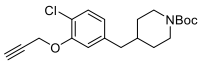

4 (1 eq, 345 mg, 1.06 mmol) and K_2CO_3 (2.2 eq, 321 mg, 2.32 mmol) were dissolved in dry DMF (10 mL) and stirred for 0.5 h. Propargyl bromide (2.2 eq, 248 µL, 2.30 mmol) was added carefully and the mixture was stirred for 48 h. When TLC analysis confirmed full conversion water and the mixture was extracted with EtOAc. The combined organic layers were washed with water and brine, dried over $MgSO_4$, filtrated and concentrated *in vacuo*. Flash column chromatography (0 → 30% EtOAc in pentane) afforded the title compound as colorless oil (381 mg, 1.05 mmol, quant.).
^{1}H NMR (400 MHz, $CDCl_3$) δ 7.27 (d, *J* = 8.0 Hz, 1H), 6.86 (d, *J* = 1.8 Hz, 1H), 6.73 (dd, *J* = 8.0, 1.8 Hz, 1H), 4.78 (d, *J* = 2.4 Hz, 2H), 4.07 (dt, *J* = 13.3, 2.6 Hz, 2H), 2.63 (td, *J* = 13.3, 2.2 Hz, 2H), 2.54 (t, *J* = 2.4 Hz, 1H), 2.52 (d, *J* = 6.9 Hz, 2H), 1.71 – 1.57 (m, 3H), 1.45 (s, 9H), 1.14 (qd, *J* = 13.1, 4.6 Hz, 2H).
^{13}C NMR (101 MHz, $CDCl_3$) δ 154.97, 152.82, 140.32, 130.18, 123.24, 120.92, 115.52, 79.44, 78.21, 76.27, 58.25, 56.89, 44.03, 42.99, 38.26, 32.00, 28.59.

4-(4-Chloro-3-(prop-2-yn-1-yloxy)benzyl)piperidin-1-ium 2,2,2-trifluoroacetate (8)

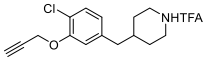

Trifluoroacetic acid (10 eq, 445 µL, 4.48 mmol) was added dropwise to an ice-cold solution of **7** (1 eq, 163 mg, 0.45 mmol) in dry DCM (20 mL), after which the mixture was allowed to warm to RT and stirred for 21 h. When TLC analysis confirmed complete conversion, all volatiles were removed under reduced pressure, affording the title compound without further purification.

3-((4-Methoxybenzyl)thio)-1*H*-1,2,4-triazole (11)

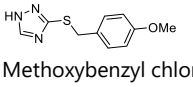

1*H*-1,2,4-triazole-3-thiol (**9**, 1.1 eq, 1.01 g, 9.99 mmol) and K_2CO_3 (1.1 eq, 1.4 g, 10 mmol) were dissolved in dry DMF (20 mL) and stirred for 0.5 h. 4-Methoxybenzyl chloride (**10**, 1 eq, 1.2 mL, 8.9 mmol) was added dropwise and the mixture was stirred for 5 h. EtOAc and water were added and the layers were separated. The aqueous layer was extracted with EtOAc, after which the combined organic layers were washed with water and brine, dried over $MgSO_4$, filtrated and concentrated *in vacuo*. The residue was dissolved in a small amount of EtOAc and put at −30°C for 7 days, affording part of the title compound as white crystals (514 mg, 2.32 mmol, 23%) while the remaining residue was stored.
^{1}H NMR (400 MHz, $CDCl_3$) δ 13.68 (bs, 1H), 8.15 (s, 1H), 7.23 – 7.14 (m, 2H), 6.80 – 6.69 (m, 2H), 4.28 (s, 2H), 3.70 (s, 3H).
^{13}C NMR (101 MHz, $CDCl_3$) δ 158.93, 147.07, 130.02, 128.54, 113.96, 55.18, 37.01.

3-((4-Methoxybenzyl)sulfonyl)-1*H*-1,2,4-triazole (12)

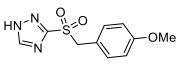

AcOOH (5 eq, 2.2 mL 35–40% in AcOH, 11.6 mmol) was added dropwise to an ice-cold solution of **11** (1 eq, 514 mg, 2.32 mmol) in dry DCM, after which the mixture was allowed to warm to RT and stirred overnight. When TLC analysis confirmed complete conversion, volatiles were removed under reduced pressure. Flash column chromatography (50 → 100% EtOAc in pentane) afforded the title compound as light brown crystals (532 mg, 2.10 mmol, 90%).

^{1}H NMR (400 MHz, MeOD) δ 8.67 (s, 1H), 7.18 – 7.10 (m, 2H), 6.87 – 6.78 (m, 2H), 4.62 (s, 2H), 3.75 (s, 3H).

^{13}C NMR (101 MHz, MeOD) δ 161.69, 146.95, 133.43, 120.16, 115.03, 61.05, 55.70.

References

1. Barglow, K. T. & Cravatt, B. F. Discovering disease-associated enzymes by proteome reactivity profiling. *Chem. Biol.* **11**, 1523–1531 (2004).
2. Satyanarayana, A. & Kaldis, P. Mammalian cell-cycle regulation: Several cdks, numerous cyclins and diverse compensatory mechanisms. *Oncogene* **28**, 2925–2939 (2009).
3. Schuster, A. *et al.* RNAi/CRISPR Screens: from a Pool to a Valid Hit. *Trends Biotechnol.* **37**, 38–55 (2019).
4. Weiss, W. A., Taylor, S. S. & Shokat, K. M. Recognizing and exploiting differences between RNAi and small-molecule inhibitors. *Nat. Chem. Biol.* **3**, 739–744 (2007).
5. Mock, E. D. *et al.* Discovery of a NAPE-PLD inhibitor that modulates emotional behavior in mice. *Nat. Chem. Biol.* **16**, 667–675 (2020).
6. Knight, Z. A. & Shokat, K. M. Chemical Genetics: Where Genetics and Pharmacology Meet. *Cell* **128**, 425–430 (2007).
7. Ogasawara, D. *et al.* Selective blockade of the lyso-PS lipase ABHD12 stimulates immune responses *in vivo*. *Nat. Chem. Biol.* **14**, 1099–1108 (2018).
8. Simon, G. M., Niphakis, M. J. & Cravatt, B. F. Determining target engagement in living systems. *Nature Chemical Biology* **9**, 200–205 (2013).
9. Jost, M. & Weissman, J. S. CRISPR Approaches to Small Molecule Target Identification. *ACS Chemical Biology* **13**, 366–375 (2018).
10. Schürmann, M., Janning, P., Ziegler, S. & Waldmann, H. Small-Molecule Target Engagement in Cells. *Cell Chem. Biol.* **23**, 435–441 (2016).
11. Wagner, J. A. Strategic approach to fit-for-purpose biomarkers in drug development. *Annu. Rev. Pharmacol. Toxicol.* **48**, 631–651 (2008).
12. Durham, T. B. & Blanco, M. J. Target Engagement in Lead Generation. *Bioorg. Med. Chem. Lett.* **25**, 998–1008 (2015).
13. Grimwood, S. & Hartig, P. R. Target site occupancy: Emerging generalizations from clinical and preclinical studies. *Pharmacol. Ther.* **122**, 281–301 (2009).
14. Willems, L. I., Overkleeft, H. S. & Van Kasteren, S. I. Current developments in activity-based protein profiling. *Bioconjug. Chem.* **25**, 1181–1191 (2014).
15. Niphakis, M. J. & Cravatt, B. F. Enzyme Inhibitor Discovery by Activity-Based Protein Profiling. *Annu. Rev. Biochem.* **83**, 341–377 (2014).
16. Adam, G. C., Sorensen, E. J. & Cravatt, B. F. Proteomic profiling of mechanistically distinct enzyme classes using a common chemotype. *Nat. Biotechnol.* **20**, 805–809 (2002).
17. Cravatt, B. F., Wright, A. T. & Kozarich, J. W. Activity-based protein profiling: From enzyme chemistry to proteomic chemistry. *Annu. Rev. Biochem.* **77**, 383–414 (2008).
18. Janssen, A. P. A. *et al.* Development of a Multiplexed Activity-Based Protein Profiling Assay to Evaluate Activity of Endocannabinoid Hydrolase Inhibitors. *ACS Chem. Biol.* **13**, 2406–2413 (2018).
19. Van Esbroeck, A. C. M. *et al.* Activity-based protein profiling reveals off-target proteins of the FAAH inhibitor BIA 10-2474. *Science* **356**, 1084–1087 (2017).
20. Verdoes, M. *et al.* A Fluorescent Broad-Spectrum Proteasome Inhibitor for Labeling Proteasomes *In Vitro* and *In Vivo*. *Chem. Biol.* **13**, 1217–1226 (2006).
21. Baggelaar, M. P. *et al.* Development of an activity-based probe and in silico design reveal highly selective inhibitors for diacylglycerol lipase-α in brain. *Angew. Chemie - Int. Ed.* **52**, 12081–12085 (2013).

22. Hussain, Z. *et al.* Phosphatidylserine-stimulated production of *N*-acyl-phosphatidylethanolamines by Ca^{2+}-dependent *N*-acyltransferase. *Biochim. Biophys. Acta - Mol. Cell Biol. Lipids* **1863**, 493–502 (2018).
23. Ghosh, M., Tucker, D. E., Burchett, S. A. & Leslie, C. C. Properties of the Group IV phospholipase A2 family. *Prog. Lipid Res.* **45**, 487–510 (2006).
24. Leslie, C. C. Cytosolic phospholipase A2: Physiological function and role in disease. *J. Lipid Res.* **56**, 1386–1402 (2015).
25. Murakami, M. *et al.* Recent progress in phospholipase A2 research: From cells to animals to humans. *Prog. Lipid Res.* **50**, 152–192 (2011).
26. Capestrano, M. *et al.* Cytosolic phospholipase $A_2\varepsilon$ drives recycling through the clathrin-independent endocytic route. *J. Cell Sci.* **127**, 977–993 (2014).
27. Wang, H. *et al.* Structure of Human GIVD Cytosolic Phospholipase A2 Reveals Insights into Substrate Recognition. *J. Mol. Biol.* **428**, 2769–2779 (2016).
28. Ogura, Y., Parsons, W. H., Kamat, S. S. & Cravatt, B. F. A calcium-dependent acyltransferase that produces *N*-Acyl phosphatidylethanolamines. *Nat. Chem. Biol.* **12**, 669–671 (2016).
29. Gillum, M. P. *et al.* *N*-acylphosphatidylethanolamine, a Gut-Derived Circulating Factor Induced by Fat Ingestion, Inhibits Food Intake. *Cell* **135**, 813–824 (2008).
30. Shiratsuchi, A. *et al.* Inhibitory effect of *N*-palmitoylphosphatidylethanolamine on macrophage phagocytosis through inhibition of Rac1 and Cdc42. *J. Biochem.* **145**, 43–50 (2008).
31. Swamy, M. J., Tarafdar, P. K. & Kamlekar, R. K. Structure, phase behaviour and membrane interactions of *N*-acylethanolamines and *N*-acylphosphatidylethanolamines. *Chem. Phys. Lipids* **163**, 266–279 (2010).
32. Domingo, J. C., Mora, M. & Africa de Madariaga, M. Incorporation of *N*-acylethanolamine phospholipids into egg phosphatidylcholine vesicles: characterization and permeability properties of the binary systems. *Biochim. Biophys. Acta - Biomembr.* **1148**, 308–316 (1993).
33. Shangguan, T., Pak, C. C., Ali, S., Janoff, A. S. & Meers, P. Cation-dependent fusogenicity of an *N*-acyl phosphatidylethanolamine. *Biochim. Biophys. Acta* **1368**, 171–183 (1998).
34. Hussain, Z., Uyama, T., Tsuboi, K. & Ueda, N. Mammalian enzymes responsible for the biosynthesis of *N*-acylethanolamines. *Biochimica et Biophysica Acta - Molecular and Cell Biology of Lipids* **1862**, 1546–1561 (2017).
35. Tsuboi, K. *et al.* Enzymatic formation of *N*-acylethanolamines from *N*-acylethanolamine plasmalogen through *N*-acylphosphatidylethanolamine-hydrolyzing phospholipase D-dependent and -independent pathways. *Biochim. Biophys. Acta - Mol. Cell Biol. Lipids* **1811**, 565–577 (2011).
36. Leung, D., Saghatelian, A., Simon, G. M. & Cravatt, B. F. Inactivation of *N*-Acyl phosphatidylethanolamine phospholipase D reveals multiple mechanisms for the biosynthesis of endocannabinoids. *Biochemistry* **45**, 4720–4726 (2006).
37. Sun, Y. X. *et al.* Biosynthesis of anandamide and *N*-palmitoylethanolamine by sequential actions of phospholipase A2 and lysophospholipase D. *Biochem. J.* **380**, 749–756 (2004).
38. Simon, G. M. & Cravatt, B. F. Endocannabinoid biosynthesis proceeding through glycero-phospho-*N*-acyl ethanolamine and a role for α/β-hydrolase 4 in this pathway. *J. Biol. Chem.* **281**, 26465–26472 (2006).
39. Simon, G. M. & Cravatt, B. F. Anandamide biosynthesis catalyzed by the phosphodiesterase GDE1 and detection of glycerophospho-*N*-acyl ethanolamine precursors in mouse brain. *J. Biol. Chem.* **283**, 9341–9349 (2008).

40. Tsuboi, K., Uyama, T., Okamoto, Y. & Ueda, N. Endocannabinoids and related *N*-acylethanolamines: biological activities and metabolism. *Inflamm. Regen.* **38**, (2018).
41. Hansen, H. S. & Vana, V. Non-endocannabinoid *N*-acylethanolamines and 2-monoacylglycerols in the intestine. *Br. J. Pharmacol.* **176**, 1443–1454 (2019).
42. Katona, I. & Freund, T. F. Multiple Functions of Endocannabinoid Signaling in the Brain. *Annu. Rev. Neurosci.* **35**, 529–558 (2012).
43. Lutz, B., Marsicano, G., Maldonado, R. & Hillard, C. J. The endocannabinoid system in guarding against fear, anxiety and stress. *Nat. Rev. Neurosci.* **16**, 705–718 (2015).
44. Mattace Raso, G., Russo, R., Calignano, A. & Meli, R. Palmitoylethanolamide in CNS health and disease. *Pharmacol. Res.* **86**, 32–41 (2014).
45. Petrosino, S. & Di Marzo, V. The pharmacology of palmitoylethanolamide and first data on the therapeutic efficacy of some of its new formulations. *Br. J. Pharmacol.* **174**, 1349–1365 (2017).
46. Dalle Carbonare, M. *et al.* A saturated *N*-acylethanolamine other than *N*-palmitoyl ethanolamine with anti-inflammatory properties: A neglected story... *J. Neuroendocrinol.* **20**, 26–34 (2008).
47. Fu, J. *et al.* Oleylethanolamide regulates feeding and body weight through activation of the nuclear receptor PPAR-α. *Nature* **425**, 90–93 (2003).
48. Gillet, L. C. J. *et al.* In-cell selectivity profiling of serine protease inhibitors by activity-based proteomics. *Mol. Cell. Proteomics* **7**, 1241–1253 (2008).
49. Speers, A. E., Adam, G. C. & Cravatt, B. F. Activity-Based Protein Profiling *In Vivo* Using a Copper(I)-Catalyzed Azide-Alkyne [3 + 2] Cycloaddition. *J. Am. Chem. Soc.* **125**, 4686–4687 (2003).
50. Binte Mustafiz, S. S. *et al.* The role of intracellular anionic phospholipids in the production of *N*-acyl-phosphatidylethanolamines by cytosolic phospholipase $A_2\varepsilon$. *J. Biochem.* **165**, 343–352 (2019).
51. van der Veen, J. N. *et al.* The critical role of phosphatidylcholine and phosphatidylethanolamine metabolism in health and disease. *Biochim. Biophys. Acta - Biomembr.* **1859**, 1558–1572 (2017).
52. Natarajan, V., Schmid, P. C. & Schmid, H. H. O. *N*-Acylethanolamine phospholipid metabolism in normal and ischemic rat brain. *Biochim. Biophys. Acta - Lipids Lipid Metab.* **878**, 32–41 (1986).
53. Epps, D. E., Natarajan, V., Schmid, P. C. & Schmid, H. H. O. Accumulation of *N*-acylethanolamine glycerophospholipids in infarcted myocardium. *Biochim. Biophys. Acta - Lipids Lipid Metab.* **618**, 420–430 (1980).
54. Moesgaard, B., Petersen, G., Jaroszewski, J. W. & Hansen, H. S. Age dependent accumulation of *N*-acyl-ethanolamine phospholipids in ischemic rat brain: A ^{31}P NMR and enzyme activity study. *J. Lipid Res.* **41**, 985–990 (2000).
55. Jin, X. H. *et al.* cDNA cloning and characterization of human and mouse Ca^{2+}-independent phosphatidylethanolamine *N*-acyltransferases. *Biochim. Biophys. Acta - Mol. Cell Biol. Lipids* **1791**, 32–38 (2009).
56. Akiyama, H. *et al.* Molecular cloning and biological activity of a novel Ha-Ras suppressor gene predominantly expressed in skeletal muscle, heart, brain, and bone marrow by differential display using clonal mouse EC cells, ATDC5. *J. Biol. Chem.* **274**, 32192–32197 (1999).
57. Schievella, A. R., Regier, M. K., Smith, W. L. & Lin, L. L. Calcium-mediated translocation of cytosolic phospholipase A_2 to the nuclear envelope and endoplasmic reticulum. *J. Biol. Chem.* **270**, 30749–30754 (1995).
58. Glover, S., Bayburt, T., Jonas, M., Chi, E. & Gelb, M. H. Translocation of the 85-kDa phospholipase A_2 from cytosol to the nuclear envelope in rat basophilic leukemia cells stimulated with calcium ionophore or IgE/antigen. *J. Biol. Chem.* **270**, 15359–15367 (1995).

59. Evans, J. H., Spencer, D. M., Zweifach, A. & Leslie, C. C. Intracellular Calcium Signals Regulating Cytosolic Phospholipase A_2 Translocation to Internal Membranes. *J. Biol. Chem.* **276**, 30150–30160 (2001).
60. Ohto, T., Uozumi, N., Hirabayashi, T. & Shimizu, T. Identification of novel cytosolic phospholipase A_2s, murine cPLA$_2$δ, ε, and ζ, which form a gene cluster with cPLA$_2$β. *J. Biol. Chem.* **280**, 24576–24583 (2005).